

BYPASSING GRADIENTS RE-PROJECTION WITH EPISODIC MEMORIES IN ONLINE CONTINUAL LEARNING

Yu Chen
University of Bristol
yc14600@bristol.ac.uk

Tom Diethe
Amazon
tdiethe@amazon.com

Peter Flach
University of Bristol
Peter.Flach@bristol.ac.uk

ABSTRACT

The use of episodic memories in continual learning is an efficient way to prevent the phenomenon of *catastrophic forgetting*. In recent studies, several gradient-based approaches have been developed to make more efficient use of compact episodic memories, which constrain the gradients resulting from new samples with gradients from memorized samples. In this paper, we propose a method for decreasing the diversity of gradients through an auxiliary optimization objective that we call Discriminative Representation Loss, instead of directly re-projecting the gradients. Our methods show promising performance with relatively cheap computational cost on several benchmark experiments.

1 INTRODUCTION

In the real world, we are often faced with situations where data distributions are shifting over time, and we would like to update our models by data we have never seen before, with bounded growth in system size. These situations fall under the umbrella of “continual learning”, which has many practical applications, such as recommender systems, retail supply chain optimization, and robotics (Lesort et al., 2019; Diethe et al., 2018; Tian et al., 2018). Similarities have also been made with the way that humans are able to learn new tasks without forgetting previously learned ones, using common knowledge shared across different skills. The fundamental problem in continual learning is *catastrophic forgetting* (McCloskey & Cohen, 1989; Kirkpatrick et al., 2017), *i.e.* (neural network) models tend to forget previously learned tasks while learning new ones.

There are two main categories of methods for alleviating forgetting in continual learning: *i)* preserving parameters of previous tasks, including methods for parameter regularization (Kirkpatrick et al., 2017; Zenke et al., 2017; Nguyen et al., 2018) and methods for incrementally evolving the model (Schwarz et al., 2018; Hung et al., 2019); *ii)* preserving the knowledge of data distributions of previous tasks, including replay-based methods (Shin et al., 2017; Rolnick et al., 2019), methods for generating compact episodic memories (Chen et al., 2018; Aljundi et al., 2019), and methods using episodic memories to refine gradients when updating model parameters (Lopez-Paz & Ranzato, 2017; Chaudhry et al., 2019b; Riemer et al., 2019).

Gradient-based approaches using episodic memories, in particular, have been receiving increasing attention. The essential idea is to use gradients produced by samples from episodic memories to constrain the gradients produced by new samples, *e.g.* by ensuring the inner product of the pair of gradients is non-negative (Lopez-Paz & Ranzato, 2017) as follows:

$$\langle g_t, g_k \rangle = \left\langle \frac{\partial \mathcal{L}(x_t, \theta)}{\partial \theta}, \frac{\partial \mathcal{L}(x_k, \theta)}{\partial \theta} \right\rangle \geq 0, \forall k < t \quad (1)$$

where t and k are time indices, x_t denotes a new sample from the current task, and x_k denotes a sample from the episodic memory. Thus, the updates of parameters are forced to preserve the performance on previous tasks as much as possible.

In Gradient Episodic Memory (GEM) Lopez-Paz & Ranzato (2017), g_t is projected to a direction that closest to it in L_2 -norm whilst also satisfying Eq. (1):

$$\min_{\tilde{g}} \frac{1}{2} \|g_t - \tilde{g}\|_2^2, \quad s.t. \langle \tilde{g}, g_k \rangle \geq 0, \quad \forall k < t \quad (2)$$

Optimization of this objective requires a high-dimensional quadratic program and thus is computationally expensive. Averaged-GEM (A-GEM) Chaudhry et al. (2019a) alleviates the computational burden of GEM by using the averaged gradient over a batch of samples instead of individual gradients of samples in the episodic memory. This not only simplifies the computation, but also obtains comparable performance with GEM. Meta-Experience Replay (MER) (Riemer et al., 2019) integrates the inner product of gradients into the loss function through a Reptile (Nichol & Schulman, 2018) style algorithm, which was originally formulated for the purposes of meta-learning. Orthogonal Gradient Descent (OGD) (Farajtabar et al., 2019) projects g_t to the direction that is perpendicular to the surface formed by $\{g_k | k < t\}$. Finally, Aljundi et al. (2019) propose Gradient-based Sample Selection (GSS), which selects samples that produce gradients with maximum diversity to store in episodic memory. Here diversity is measured by the cosine similarity between gradients. Since the cosine similarity is computed using the inner product of two normalized gradients, GSS embodies the same principle as other gradient-based approaches with episodic memories. Although GSS suggests the samples with most diverse gradients are important to the generalization across tasks, Chaudhry et al. (2019b) show that the average gradient over a small set of random samples may be able to obtain good generalization as well.

In this paper, we answer the following questions: *i*) Which samples tend to produce diverse gradients that strongly conflict with other samples? *ii*) Why are such samples able to help with generalization? *iii*) Why does a small set of randomly chosen samples also help with generalization? Based on our findings when answering these questions, we propose a new auxiliary objective, Discriminative Representation Loss (DRL), for classification tasks in online continual learning. In addition, we suggest a simple replay method Balanced Experience Replay (BER) as an alternative to Experience Replay (ER) that, we will show, naturally complements DRL and outperforms other methods by itself in several cases. Our methods show improved performance with relatively low computational cost when compared to several state-of-the-art methods across multiple benchmark tasks in the setting of online continual learning.

2 A NEW PERSPECTIVE OF REDUCING GRADIENT DIVERSITY

According to Eq. (1), larger cosine similarities between gradients produced by current and previous tasks result in improved generalisation. This in turn indicates that samples that lead to the most diverse gradients provide the most difficulty during learning. This can be interpreted from the perspective of constrained optimization as discussed in Aljundi et al. (2019). Moreover, the diversity of gradients relates to the Gradient Signal to Noise Ratio (GSNR) (Liu et al., 2020), which plays a crucial role in the model’s generalization ability. Intuitively, when more of the gradients point in the same direction, the variance will be smaller, leading to a larger GSNR, and consequently, improved test-time performance. In this sense, reducing the diversity of gradients may improve the generalization ability of models.

2.1 WHICH SAMPLES PRODUCE DIVERSE GRADIENTS?

We conducted a simple experiment on classification tasks of 2-D Gaussian distributions, and tried to identify diverse samples in the 2-D feature space. We trained a linear model on the first task to discriminate between two classes (blue and orange dots in Fig. 1a). We then applied the algorithm Gradient-based Sample Selection with Integer Quadratic Programming (GSS-IQP) (Aljundi et al., 2019) to select 10% of the samples of training data that produce gradients with the lowest similarity (black dots in Fig. 1a), and denote this set of samples as $\widehat{M} = \min_M \sum_{i,j \in M} \frac{\langle g_i, g_j \rangle}{\|g_i\| \cdot \|g_j\|}$. It is clear from Fig. 1a that the samples in \widehat{M} are mostly around the decision boundary between the two classes, while a small number are from the region furthest from class centres. Increasing the size of \widehat{M} results in the inclusion of samples that trace the outer edges of the data distributions from each class. Clearly the gradients can be strongly opposed when samples from different classes are very similar. Samples close to decision boundaries are most likely to exhibit this characteristic.

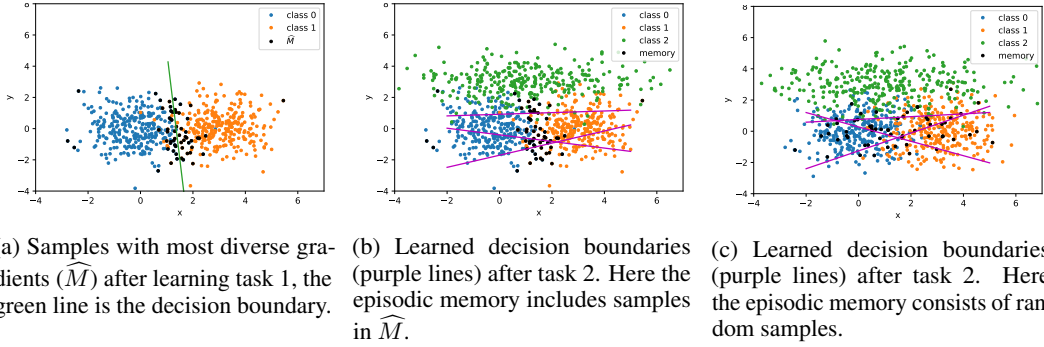


Figure 1: 2-dimensional classification examples, the x and y axis are the coordinates (also features) of samples. We sequentially train a logistic regression model on two tasks: the first task is to classify two classes as shown in (a); the second class is to incrementally classify a third class as shown in (b) and (c). The solid lines are decision boundaries between classes.

Intuitively, storing the decision boundaries of previously learned classes should be an efficient way to preserve classification performance on those classes. However, if the episodic memory only includes samples representing the learned boundaries, it may miss important information when the model is required to incrementally learn new classes. We show this by introducing a second task - training the model above on a third class. Figs. 1b and 1c displays the decision boundaries (which split the feature space in a one vs. all manner) learned by the model after task 2 with \widehat{M} (Fig. 1b) and a random set of samples (Fig. 1c) from task 1 as the episodic memory. The random episodic memory shows better performance than the one selected by GSS-IQP, since the new decision boundaries rely on samples not included in \widehat{M} . According to this finding, we would prefer the episodic memory not to be biased to boundaries describing a small region of the data distribution of previous tasks. Ideally, with \widehat{M} large enough, the model can remember all boundaries of each class, and hence learn much more accurate decision boundaries in subsequent tasks. However, memory size may be limited in practice, especially for high-dimensional data.

So far, the empirical results show that diversity of gradients relate to the diversity of representations: 1). less diverse representations in the same class result in less diverse gradients; 2). less diverse representations in different classes result in more diverse gradients. Now we make a formal connection between the diversity of gradients and representations for the linear model, proofs are provided in Appx. A. **Notations:** Let \mathcal{L} represent the loss function. $\mathbf{W} \in \mathbb{R}^{D \times K}$ is the weight matrix, and $\mathbf{x} \in \mathbb{R}^D$ denotes the input data features, $\mathbf{y} \in \mathbb{R}^K$ denotes the label of \mathbf{x} , D is the number of features, K is the number of classes, the gradient $\mathbf{g}_n = \nabla_{\mathbf{W}} \mathcal{L}(\mathbf{x}_n, \mathbf{y}_n)$.

Theorem 1. When \mathcal{L} is the softmax cross entropy loss, $\langle \mathbf{g}_n, \mathbf{g}_m \rangle \neq 0$, and $\mathbf{y}_n \neq \mathbf{y}_m$, let $\mathbf{p}_n = \text{softmax}(\mathbf{o}_n)$, $\mathbf{o}_n = \mathbf{W}\mathbf{x}_n$, c_n denotes the class index of \mathbf{x}_n (i.e. $\mathbf{y}_{n,c_n} = 1$). Suppose $\alpha = \mathbf{p}_{n,c_m} + \mathbf{p}_{m,c_n}$ and $\delta = \|\mathbf{p}_n - \mathbf{p}_m\|^2$ are random variables, then:

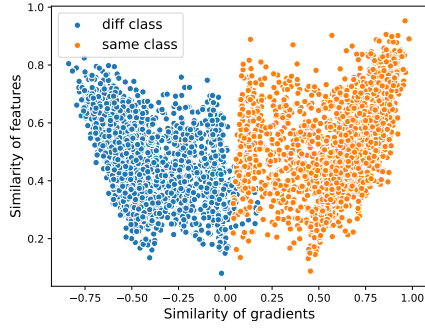
$$P(\text{sign}(\langle \mathbf{g}_n, \mathbf{g}_m \rangle) = \text{sign}(-\langle \mathbf{x}_n, \mathbf{x}_m \rangle)) \geq P(\delta > 2(1 - \alpha)),$$

By Theorem 1, we can see why two samples from two different classes and close to the decision boundary are tend to produce diverse gradients. In such a case, $\langle \mathbf{x}_n, \mathbf{x}_m \rangle$ is likely positive, α is close to or even larger than 1, since $\delta \geq 0$, it will result in $\delta > 2(1 - \alpha)$ in a high probability. We demonstrate the distribution of $\langle \mathbf{g}_n, \mathbf{g}_m \rangle$ in several scenarios in Fig. 6 in Appx. A.

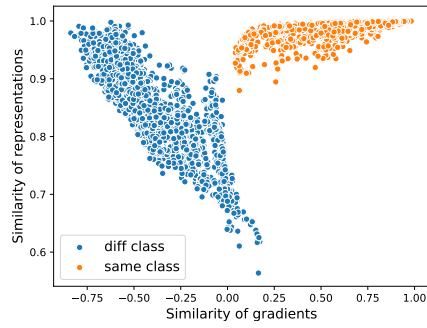
Theorem 2. When \mathcal{L} is the softmax cross entropy loss, $\langle \mathbf{g}_n, \mathbf{g}_m \rangle \neq 0$, and $\mathbf{y}_n = \mathbf{y}_m$, then:

$$\text{sign}(\langle \mathbf{g}_n, \mathbf{g}_m \rangle) = \text{sign}(\langle \mathbf{x}_n, \mathbf{x}_m \rangle),$$

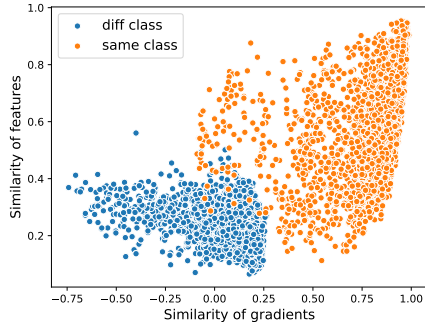
Theorem 2 indicates $\langle \mathbf{g}_n, \mathbf{g}_m \rangle$ can be negative only if $\langle \mathbf{x}_n, \mathbf{x}_m \rangle$ is negative when the two samples from the same class. Theorems 1 and 2 give the explicit connection between the diversity of gradients and representations for a linear model. It is a non-trivial work to show a similar theoretical results for general neural networks and we leave it as a future work. In the following we will show empirical study of neural networks trained by high dimensional data.



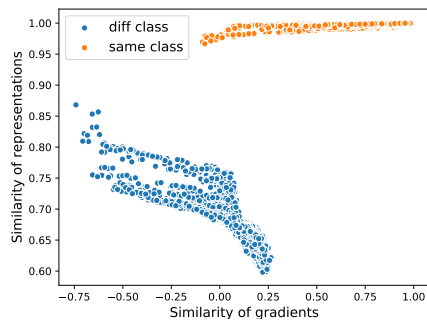
(a) Similarities of gradients vs. features (class 7 & 9)



(b) Similarities of gradients vs. representations (class 7 & 9)



(c) Similarities of gradients vs. features (class 0 & 1)



(d) Similarities of gradients vs. representations (class 0 & 1)

Figure 2: Similarities of gradients, features and representations of two classes in MNIST dataset. The x axis is the cosine similarity of gradients, the y axis is the cosine similarity of features in (a) and (c), and representations in (b) and (d). Blue dots indicate the similarity between two samples from two different classes, while orange dots indicate that the two samples are from the same class.

The key for a model to be able to successfully learn accurate decision boundaries is to find the right signal that can clearly discriminate different classes. We can assume that this signal is present after transformation from the original feature space to the model embedding space. According to the above findings, we would expect the similarity of representations to have correlations with the similarity of gradients. We have conducted another experiment on MNIST (LeCun et al., 2010) dataset to verify this assumption.

We first trained two binary classifiers for two groups of MNIST classes ($\{0, 1\}$ and $\{7, 9\}$). The classifiers have two hidden layers each with 100 hidden units. We randomly chose 100 test samples from each group, and computed the pairwise cosine similarities of gradients, features and representations after the model is trained. *Representations are obtained by concatenating the output of all layers of the neural network, including the final layer. Features are the raw input space of data.* We display the different similarities in Fig. 2, where blue dots indicate the similarity between two samples from two different classes, while orange dots indicate that the two samples are from the same class. In Figs. 2a and 2c, the correlation coefficients of blue dots are -0.37 and -0.38, which of orange dots are 0.38 and 0.36. In Figs. 2b and 2d, the correlation coefficients of blue dots are -0.86 and -0.85, which of orange dots are 0.71 and 0.79. In all cases, the similarities of representations show stronger correlations with the similarities of gradients than those of features. This is especially true when the compared samples are from different classes (blue dots in Fig. 2): here larger similarities of representations correspond to smaller similarities of gradients. These results obviously align with the results of linear models. In addition, the blue and orange dots are perfectly separable on the y axis in Fig. 2d, which indicates that the classifier for class 0 and 1 has learnt strongly discriminative representations, and as a result achieves nearly perfect (99.95%) accuracy on the test set. In comparison, the classifier for class 7 and 9 has learnt less discriminative representations, resulting in lower test accuracy (96.25%).

2.2 DISCRIMINATIVE REPRESENTATION LOSS

Through the above section we show that the discrimination ability of representations strongly correlates with the diversity of gradients, and more discriminative representations lead to more consistent gradients. We use this insight to introduce an extra objective Discriminative Representation Loss (DRL) into the optimization objective of classification tasks in continual learning. Instead of explicitly re-projecting gradients during training process, DRL helps with decreasing gradient diversity by optimizing the representations. As defined in Eq. (3), DRL consists of two parts: one is for minimizing the similarities of representations between samples from different classes (\mathcal{L}_{bt}), the other is for maximizing the similarities of representations between samples from a same class (\mathcal{L}_{wi}).

$$\min_{\Theta} \mathcal{L}_{DR} = \min_{\Theta} (\mathcal{L}_{bt} - \mathcal{L}_{wi}),$$

$$\mathcal{L}_{bt} = \frac{1}{B_{bt}} \sum_{l=1}^L \sum_{i=1}^B \sum_{j=1, y_j \neq y_i}^B \langle h_{l,i}, h_{l,j} \rangle, \quad \mathcal{L}_{wi} = \frac{1}{B_{wi}} \sum_{l=1}^L \sum_{i=1}^B \sum_{j=1, j \neq i, y_j = y_i}^B \langle h_{l,i}, h_{l,j} \rangle, \quad (3)$$

where Θ denotes the parameters of the model, L is the number of layers of the model, B is training batch size. B_{bt} and B_{wi} denote the number of pairs of samples in the training batch that are from different classes and the same class, respectively, $h_{l,i}$ is the output of layer l by input x_i and y_i is the label of x_i . Intuitively, DRL optimizes large margins between classes in a transformed feature space which is analogous to Kernel Fisher Discriminant analysis (KFD) (Mika et al., 1999) and distance metric learning (Weinberger et al., 2006) but with following major differences: *i*) DRL optimizes the transformation function (i.e. the neural network) whereas KFD and metric learning optimize the kernel in which the transformation function is implicit; *ii*) DRL is computed by a batch of samples instead of the whole dataset, and it is possible to have $\mathcal{L}_{wi} = 0$ when there are no more than one sample from a given class in that batch. In a summary, DRL bears some resemblance to KFD and metric learning, but is tailored to neural networks optimized by stochastic gradient descent.

$$\mathcal{L} = \mathcal{L}_{clf} + \lambda \mathcal{L}_{DR}, \quad \lambda > 0, \quad (4)$$

The final loss function combines the commonly used cross entropy loss for classification tasks (\mathcal{L}_{clf}) with DRL (\mathcal{L}_{DR}) as shown in Eq. (4), where λ is a hyperparameter controlling the strength of \mathcal{L}_{DR} , which is larger for increased resistance to forgetting, and smaller for greater elasticity. We observe that relatively larger λ results in improved performance for more homogeneous tasks, as there is reduced conflict between forgetting and elasticity in such cases. We verify the effect of this objective on reducing the diversity of gradients in Fig. 7 in Appx. C.

3 ONLINE MEMORY UPDATE AND BALANCED EXPERIENCE REPLAY

Here we will examine the online setting of continual learning – only training the model with one epoch on the training data – as was done for other gradient-based approaches with episodic memories (Lopez-Paz & Ranzato, 2017; Chaudhry et al., 2019a; Aljundi et al., 2019).

We update the episodic memories based on the ring buffer strategy: keep the last n_c samples of class c in the memory buffer, where n_c is the memory size of a seen class c . For fair comparisons with other methods, we have deployed two different settings for the episodic memories: *i*) the total size of the memory buffer is fixed from the first task, implying a fixed budget for the memory cost; *ii*) the memory size of each task or class is fixed, implying the memory cost linearly increases with the number of tasks. In both settings, our goal is to maintain a uniform distribution over all seen classes. However, the buffer may not be evenly allocated to each class before enough samples are acquired for newly arriving classes. This is straightforward for the second setting; we show pseudo-code of the first setting in Alg. 1 in Appx. B for a clearer explanation.

Since DRL depends on the pairwise similarities of samples in the training batch, we would prefer the training batch to include as wide a variety of different classes as possible to obtain sufficient discriminative information. Hence, we adjust the ER algorithm for the needs of DRL. The basic idea is to uniformly sample from all classes in the memory buffer to form a training batch, so that this batch is evenly distributed across all seen classes. We call this Balanced Experience Replay (BER), its pseudo code is in Alg. 2 in Appx. B. In our experiments, BER shows improved performance compared with ER in terms of forgetting.

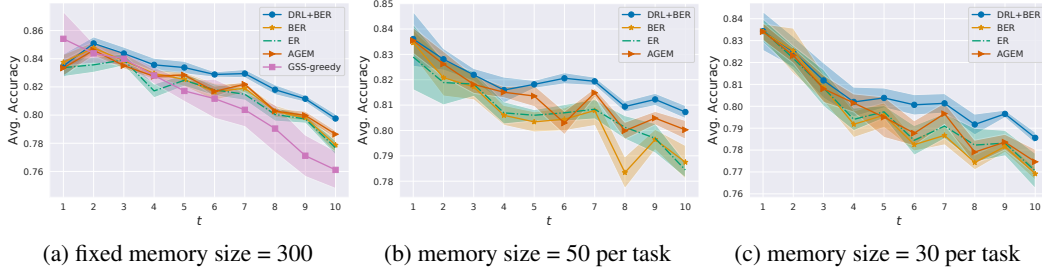


Figure 3: Average accuracy of Permuted MNIST in two different memory settings. The x axis is the index of tasks, the shaded area is plotted by standard deviation of 5 runs.

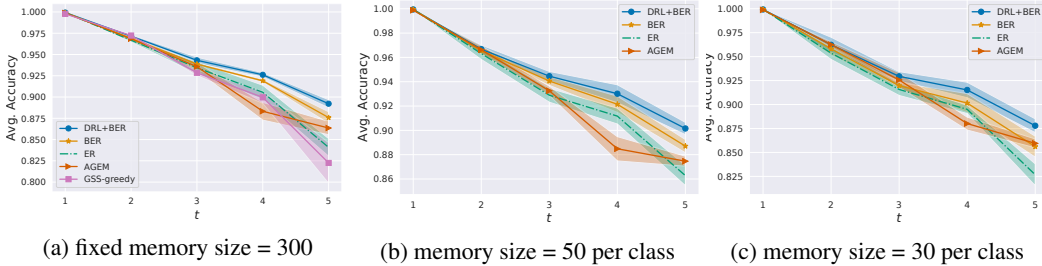


Figure 4: Average accuracy of Disjoint MNIST in two different memory settings. The x axis is the index of tasks, the shaded area is plotted by standard deviation of 5 runs.

Table 1: Average forgetting of MNIST tasks with incremental memory size.

	DRL+BER	BER	ER	A-GEM
Permuted MNIST (50/task)	0.038 ± 0.001	0.047 ± 0.003	0.056 ± 0.005	0.048 ± 0.005
Permuted MNIST (30/task)	0.053 ± 0.004	0.064 ± 0.004	0.072 ± 0.006	0.067 ± 0.006
Disjoint MNIST (50/class)	0.071 ± 0.006	0.082 ± 0.006	0.133 ± 0.009	0.102 ± 0.007
Disjoint MNIST (30/class)	0.109 ± 0.011	0.134 ± 0.015	0.182 ± 0.015	0.124 ± 0.004

Table 2: Average forgetting of MNIST tasks with fixed memory size 300.

	DRL+BER	BER	ER	A-GEM	GSS-greedy
Permuted MNIST	0.052 ± 0.003	0.064 ± 0.007	0.069 ± 0.005	0.053 ± 0.004	0.093 ± 0.016
Disjoint MNIST	0.085 ± 0.007	0.1 ± 0.007	0.161 ± 0.013	0.116 ± 0.012	0.182 ± 0.03

4 EXPERIMENTS

In this section we evaluate our methods on multiple benchmark tasks by comparing with several baseline methods in the setting of online continual learning.

Baselines: We compare our methods with following related gradient-based approaches:

A-GEM Chaudhry et al. (2019a): refines gradients using samples from episodic memory, similar to GEM Lopez-Paz & Ranzato (2017) but with lower computational cost.

ER Chaudhry et al. (2019b): “vanilla” experience replay, yet was shown to achieve better performance than A-GEM and MER Riemer et al. (2019) in the online continual learning setting. It simply composes a training batch divided equally between samples from the episodic memory and samples from the current task. We consider this as a baseline for standalone BER.

GSS-greedy Aljundi et al. (2019): based on gradient diversities for selecting samples into the episodic memory. It is a variant of GSS-IQP with lower computational cost but with similar performance. We

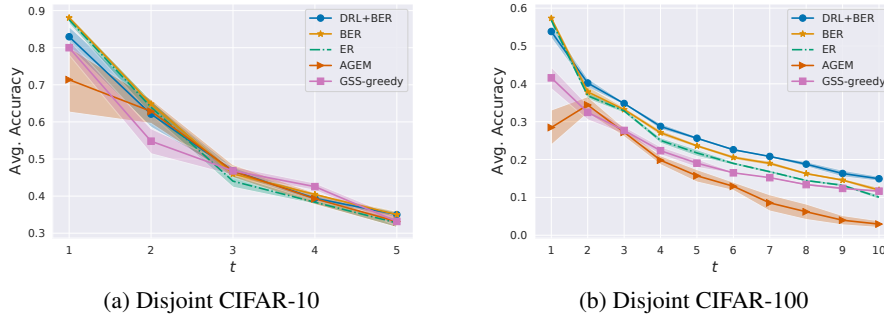


Figure 5: Average accuracy on CIFAR tasks. Memory size is fixed to 1000 for CIFAR-10 and 3000 for CIFAR-100.

Table 3: Final average accuracy on CIFAR tasks

	DRL+BER	BER	ER	A-GEM	GSS-greedy
CIFAR-10	0.35 ± 0.007	0.35 ± 0.009	0.328 ± 0.012	0.331 ± 0.016	0.332 ± 0.012
CIFAR-100	0.149 ± 0.006	0.119 ± 0.007	0.1 ± 0.006	0.029 ± 0.009	0.117 ± 0.004

Table 4: Average forgetting on CIFAR tasks

	DRL+BER	BER	ER	A-GEM	GSS-greedy
CIFAR-10	0.247 ± 0.015	0.513 ± 0.011	0.564 ± 0.015	0.307 ± 0.033	0.291 ± 0.037
CIFAR-100	0.164 ± 0.007	0.409 ± 0.004	0.469 ± 0.011	0.331 ± 0.043	0.271 ± 0.01

can only use this in comparisons with episodic memories with fixed size, since it does not consider class labels when selecting samples.

Performance measures: We use following measures to evaluate the performance of tested methods, which are commonly used for classification tasks in continual learning:

Average accuracy, which is evaluated after learning each task and measures the average accuracy over all learned tasks: $\bar{a}_t = \frac{1}{t} \sum_{i=1}^t a_{t,i}$, where t is the index of current task, $a_{t,i}$ is the accuracy of task i after learning task t .

Average forgetting (Chaudhry et al., 2018), which is evaluated after learning all tasks and measures average accuracy drop after learning the whole task sequence: $\bar{f}_T = \frac{1}{T-1} \sum_{i=1}^{T-1} \max_{j \in \{i, \dots, T-1\}} (a_{j,i} - a_{T,i})$.

Benchmark tasks: We have conducted experiments on following benchmark tasks to evaluate our methods:

Permuted MNIST: 10 tasks using the MNIST dataset, each task includes the same 10 classes with different permutation of features. The training size is 1000 samples per task;

Disjoint MNIST: 5 tasks using the MNIST dataset, each task includes two classes which are disjoint from the other tasks. The training size is 1000 samples per task;

Disjoint CIFAR-10: 5 tasks using the CIFAR-10 dataset (Krizhevsky et al., 2009), each task includes two classes which are disjoint from other tasks. The training size is 2000 samples per task;

Disjoint CIFAR-100: 10 tasks using the CIFAR-100 dataset (Krizhevsky et al., 2009), each task includes 10 classes which are disjoint from other tasks. The training size is 5000 samples per task.

N.B.: we follow the settings in Lopez-Paz & Ranzato (2017); Aljundi et al. (2019), training the models using limited training size. Moreover, we use *single-head* (shared output) models in all of our experiments, meaning that we do not require a task indicator at testing time. Such settings are more difficult for continual learning but more practical in real applications.

Table 5: Training time (in seconds) of the whole task sequence of MNIST tasks with fixed memory size 300, which have been tested on a laptop with an 8-core Intel CPU and 32G RAM.

	DRL+BER	BER	ER	A-GEM	GSS-greedy
Permuted MNIST	12.48 ± 0.16	11.17 ± 0.18	10.38 ± 0.05	28.0 ± 0.09	33.98 ± 0.6
Disjoint MNIST	5.6 ± 0.14	5.29 ± 0.08	5.25 ± 0.02	13.41 ± 0.47	19.07 ± 1.31

Experimental settings: For tasks on MNIST dataset, we use a dense neural network with ReLU activation and two hidden layers, and each layer has 100 hidden units. For tasks on CIFAR datasets, we use the same reduced Resnet18 as used in Chaudhry et al. (2019a). We use the online setting as used by the baseline methods, meaning the model is trained for only one epoch on the training sets. The standard deviation shown in all results are evaluated over 5 runs with different random seeds. More details of experimental settings are in Appx. D.

We tested both fixed and incremental memory size on tasks using the MNIST dataset. Figs. 3 and 4 display the average accuracy after learning each task and Tabs. 1 and 2 show the average forgetting at the end of the data stream. In all of these cases our method DRL+BER outperforms the baselines in terms of both measures. In addition, the standalone BER achieves better performance on forgetting than ER. With smaller memory size, the gaps between average accuracies between these methods are reduced, but DRL still shows some improvement.

Fig. 5 displays the average accuracy of Disjoint CIFAR-10 and Disjoint CIFAR-100 with fixed memory size 1000 and 3000 respectively. For a clearer comparison, we also show their average accuracy after learning the last task in Tab. 3. For Disjoint CIFAR-10, DRL+BER and BER show similar performance on the average accuracy, and DRL + BER outperforms others on the average forgetting, as shown in Tab. 4. Disjoint CIFAR-100 is generally more difficult than other tasks, with fewer training samples per class but more classes. All methods shown serious difficulty in generalizing across the 100 classes sequentially. Here we observe a strong conflict between learning new tasks and remembering old ones. BER is the most capable at learning new tasks, while GSS-greedy is most capable at remembering the first task. A-GEM performs steadily worse in terms of both remembering and learning as more tasks are received. ER performs similarly to BER, while DRL improves remembering based on BER but is less capable of learning. We show more results in the supplementary material.

We also compare the training time of all methods on MNIST tasks in Tab. 5. The computational complexity of DRL is $O(B^2H)$, where B is training batch size, H is the dimension of representations. B is small (10 or 20 in our experiments) and $H \ll W$, commonly $B^2H \ll W$ in neural networks, where W is the dimension of parameters. In comparison, the methods which rely on inner product of gradients have at least $O(W)$ computational complexity. As shown in Tab. 5, our methods achieved their improved performance with much lower computational cost than A-GEM and GSS-greedy.

5 DISCUSSION AND CONCLUSION

The two fundamental problems of continual learning with small episodic memories are how to: (i) make the best use of a small set of samples; and (ii) construct a small set of samples that are most representative of a large dataset. Gradient based approaches have shown that the diversity of gradients computed on data from different tasks is a key to generalization over these tasks. In this paper, we show that the most diverse gradients are from samples that are close to decision boundaries. Moreover, we connect the diversity of gradients to discrimination ability of representations learned by the model, which leads to an alternative way to reduce the diversity of gradients instead of re-projecting gradients directly. Further, we point out that, by only preserving samples that depict the existing decision boundaries, important information may be lost. In most of our experiments, randomly chosen samples outperform those selected by gradient diversity. We argue that, in combination with our method, the right direction should be to preserve as much statistical information of the data distribution as possible, such as through coresets or sketches (Karnin & Liberty, 2019). We will leave this as a future work.

REFERENCES

- Rahaf Aljundi, Min Lin, Baptiste Goujaud, and Yoshua Bengio. Gradient based sample selection for online continual learning. In *Advances in Neural Information Processing Systems*, pp. 11816–11825, 2019.
- Arslan Chaudhry, Puneet K Dokania, Thalaiyasingam Ajanthan, and Philip HS Torr. Riemannian walk for incremental learning: Understanding forgetting and intransigence. In *Proceedings of the European Conference on Computer Vision (ECCV)*, pp. 532–547, 2018.
- Arslan Chaudhry, MarcAurelio Ranzato, Marcus Rohrbach, and Mohamed Elhoseiny. Efficient lifelong learning with a-GEM. In *International Conference on Learning Representations*, 2019a. URL https://openreview.net/forum?id=Hkf2_sC5FX.
- Arslan Chaudhry, Marcus Rohrbach, Mohamed Elhoseiny, Thalaiyasingam Ajanthan, Puneet K Dokania, Philip HS Torr, and Marc’Aurelio Ranzato. On tiny episodic memories in continual learning. *arXiv preprint arXiv:1902.10486*, 2019b.
- Yu Chen, Tom Diethe, and Neil Lawrence. Facilitating bayesian continual learning by natural gradients and stein gradients. *Continual Learning Workshop of 32nd Conference on Neural Information Processing Systems (NeurIPS 2018)*, 2018.
- Tom Diethe, Tom Borchert, Eno Thereska, Borja de Balle Pigem, and Neil Lawrence. Continual learning in practice. In *Continual Learning Workshop of 32nd Convergence on Neural Information Processing Systems (NeurIPS 2018)*, 2018.
- Mehrdad Farajtabar, Navid Azizan, Alex Mott, and Ang Li. Orthogonal gradient descent for continual learning. *arXiv preprint arXiv:1910.07104*, 2019.
- Ching-Yi Hung, Cheng-Hao Tu, Cheng-En Wu, Chien-Hung Chen, Yi-Ming Chan, and Chu-Song Chen. Compacting, picking and growing for unforgetting continual learning. In *Advances in Neural Information Processing Systems*, pp. 13647–13657, 2019.
- Zohar Karnin and Edo Liberty. Discrepancy, coresets, and sketches in machine learning. In *Conference on Learning Theory*, pp. 1975–1993, 2019.
- Diederik P Kingma and Jimmy Ba. Adam: A method for stochastic optimization. *arXiv preprint arXiv:1412.6980*, 2014.
- James Kirkpatrick, Razvan Pascanu, Neil Rabinowitz, Joel Veness, Guillaume Desjardins, Andrei A Rusu, Kieran Milan, John Quan, Tiago Ramalho, Agnieszka Grabska-Barwinska, et al. Overcoming catastrophic forgetting in neural networks. *Proceedings of the national academy of sciences*, pp. 201611835, 2017.
- Alex Krizhevsky, Geoffrey Hinton, et al. Learning multiple layers of features from tiny images. Technical report, Citeseer, 2009.
- Yann LeCun, Corinna Cortes, and Christopher JC Burges. MNIST handwritten digit database. *AT&T Labs [Online]*. Available: <http://yann.lecun.com/exdb/mnist>, 2, 2010.
- Timothée Lesort, Vincenzo Lomonaco, Andrei Stoian, Davide Maltoni, David Filliat, and Natalia Díaz-Rodríguez. Continual learning for robotics. *arXiv preprint arXiv:1907.00182*, 2019.
- Jinlong Liu, Yunzhi Bai, Guoqing Jiang, Ting Chen, and Huayan Wang. Understanding why neural networks generalize well through GSNR of parameters. In *International Conference on Learning Representations*, 2020. URL <https://openreview.net/forum?id=HyevIJStwH>.
- David Lopez-Paz and Marc’Aurelio Ranzato. Gradient episodic memory for continual learning. In *Advances in Neural Information Processing Systems*, pp. 6467–6476, 2017.
- Michael McCloskey and Neal J Cohen. Catastrophic interference in connectionist networks: The sequential learning problem. In *Psychology of learning and motivation*, volume 24, pp. 109–165. Elsevier, 1989.

-
- Sebastian Mika, Gunnar Ratsch, Jason Weston, Bernhard Scholkopf, and Klaus-Robert Mullers. Fisher discriminant analysis with kernels. In *Neural networks for signal processing IX: Proceedings of the 1999 IEEE signal processing society workshop (cat. no. 98th8468)*, pp. 41–48. Ieee, 1999.
- Cuong V Nguyen, Yingzhen Li, Thang D Bui, and Richard E Turner. Variational continual learning. In *International Conference on Learning Representations*, 2018.
- Alex Nichol and John Schulman. Reptile: a scalable metalearning algorithm. *arXiv preprint arXiv:1803.02999*, 2, 2018.
- Matthew Riemer, Ignacio Cases, Robert Ajemian, Miao Liu, Irina Rish, Yuhai Tu, , and Gerald Tesauro. Learning to learn without forgetting by maximizing transfer and minimizing interference. In *International Conference on Learning Representations*, 2019. URL <https://openreview.net/forum?id=BlgTShAct7>.
- David Rolnick, Arun Ahuja, Jonathan Schwarz, Timothy Lillicrap, and Gregory Wayne. Experience replay for continual learning. In *Advances in Neural Information Processing Systems*, pp. 348–358, 2019.
- Jonathan Schwarz, Jelena Luketina, Wojciech M Czarnecki, Agnieszka Grabska-Barwinska, Yee Whye Teh, Razvan Pascanu, and Raia Hadsell. Progress & compress: A scalable framework for continual learning. *arXiv preprint arXiv:1805.06370*, 2018.
- Hanul Shin, Jung Kwon Lee, Jaehong Kim, and Jiwon Kim. Continual learning with deep generative replay. In *Advances in Neural Information Processing Systems*, pp. 2990–2999, 2017.
- Huangshi Tian, Minchen Yu, and Wei Wang. Continuum: A platform for cost-aware, low-latency continual learning. In *Proceedings of the ACM Symposium on Cloud Computing*, pp. 26–40, 2018.
- Kilian Q Weinberger, John Blitzer, and Lawrence K Saul. Distance metric learning for large margin nearest neighbor classification. In *Advances in neural information processing systems*, pp. 1473–1480, 2006.
- Friedemann Zenke, Ben Poole, and Surya Ganguli. Continual learning through synaptic intelligence. In *International Conference on Machine Learning*, pp. 3987–3995, 2017.

A PROOF OF THEOREMS

Notations: Let \mathcal{L} represent the loss function, model output $\mathbf{o}_n = \mathbf{W}\mathbf{x}_n$, $\mathbf{W} \in \mathbb{R}^{D \times K}$ is the weight matrix, and $\mathbf{x} \in \mathbb{R}^D$ denotes the input data features, $\mathbf{y} \in \mathbb{R}^K$ denotes the label of \mathbf{x} , D is the number of features, K is the number of classes, the gradient $\mathbf{g}_n = \nabla_{\mathbf{W}} \mathcal{L}(\mathbf{x}_n, \mathbf{y}_n)$.

Fact 1. Suppose $(\mathbf{x}_n, \mathbf{y}_n), (\mathbf{x}_m, \mathbf{y}_m)$ are two different training samples, $\mathbf{g}_n = \partial \mathcal{L}(\mathbf{x}_n, \mathbf{y}_n) / \partial \mathbf{W}$, $\ell'_n = \partial \mathcal{L}(\mathbf{x}_n, \mathbf{y}_n) / \partial \mathbf{o}_n$, when $\langle \mathbf{g}_n, \mathbf{g}_m \rangle \neq 0$, we have:

$$\langle \mathbf{g}_n, \mathbf{g}_m \rangle = \langle \mathbf{x}_n, \mathbf{x}_m \rangle \langle \ell'_n, \ell'_m \rangle,$$

Theorem 1. When \mathcal{L} is the softmax cross entropy loss, $\langle \mathbf{g}_n, \mathbf{g}_m \rangle \neq 0$, and $\mathbf{y}_n \neq \mathbf{y}_m$, let $\mathbf{p}_n = \text{softmax}(\mathbf{o}_n)$, c_n denotes the class index of \mathbf{x}_n (i.e. $\mathbf{y}_{n, c_n} = 1$). Suppose $\alpha = \mathbf{p}_{n, c_n} + \mathbf{p}_{m, c_n}$ and $\delta = \|\mathbf{p}_n - \mathbf{p}_m\|^2$ are random variables, then:

$$P(\text{sign}(\langle \mathbf{g}_n, \mathbf{g}_m \rangle) = \text{sign}(-\langle \mathbf{x}_n, \mathbf{x}_m \rangle)) \geq P(\delta > 2(1 - \alpha)),$$

Proof. By the definition of \mathcal{L} , we can find:

$$\ell'_n = \mathbf{p}_n - \mathbf{y}_n, \quad (5)$$

As $\mathbf{y}_n \neq \mathbf{y}_m$, we have

$$\langle \ell'_n, \ell'_m \rangle = \langle \mathbf{p}_n, \mathbf{p}_m \rangle - \mathbf{p}_{n, c_n} - \mathbf{p}_{m, c_n}$$

And

$$\langle \mathbf{p}_n, \mathbf{p}_m \rangle = \frac{1}{2}(\|\mathbf{p}_n\|^2 + \|\mathbf{p}_m\|^2 - \|\mathbf{p}_n - \mathbf{p}_m\|^2) \leq \frac{1}{2}(2 - \|\mathbf{p}_n - \mathbf{p}_m\|^2)$$

which gives $\langle \ell'_n, \ell'_m \rangle \leq 1 - \frac{1}{2}\delta - \alpha$. When $\delta > 2(1 - \alpha)$, we must have $\langle \ell'_n, \ell'_m \rangle < 0$. According to Fact 1, we prove this theorem. \square

In Fig. 6, we demonstrate the distribution of the inner product $\mathcal{S}_{n, m} = \langle \ell'_n, \ell'_m \rangle$ for a 5-class classification task in several situations under the assumption that $\mathbf{p}_n, \mathbf{p}_m$ are random variables of two Dirichlet distributions, where we set $\mathbf{y}_n = (0, 0, 1, 0, 0)$, $\mathbf{y}_m = (0, 0, 0, 1, 0)$ and the model is reasonably trained: (a) $\mathbf{p}_n \sim \text{Dir}(0.05, 0.05, 0.45, 0.4, 0.05)$, $\mathbf{p}_m \sim \text{Dir}(0.05, 0.05, 0.4, 0.45, 0.05)$, it shows the scenario that two samples are close to the decision boundary of their true classes, i.e. $\mathbf{p}_n, \mathbf{p}_m$ concentrate on both classes; (b) $\mathbf{p}_n = \{0.05, 0.05, 0.8, 0.05, 0.05\}$, $\mathbf{p}_m = \{0.05, 0.05, 0.4, 0.45, 0.05\}$, it shows the scenario that $\mathbf{x}_n, \mathbf{x}_m$ are away from and close to the decision boundary, respectively; (c) $\mathbf{p}_n, \mathbf{p}_m$ are close to true labels, it shows the scenario that two samples are both away from the decision boundary. We see that the inner product of two gradients $\mathcal{S}_{n, m}$ is negative almost for sure in Fig. 6a, which explains the results in Fig. 1.

Theorem 2. When \mathcal{L} is the softmax cross entropy loss, $\langle \mathbf{g}_n, \mathbf{g}_m \rangle \neq 0$, and $\mathbf{y}_n = \mathbf{y}_m$, then:

$$\text{sign}(\langle \mathbf{g}_n, \mathbf{g}_m \rangle) = \text{sign}(\langle \mathbf{x}_n, \mathbf{x}_m \rangle),$$

Proof. Since $\sum_{k=1}^K \mathbf{p}_{n, k} = 1$ and $\mathbf{p}_{n, k} \geq 0, \forall k$, and $c_n = c_m = c$,

$$\langle \ell'_n, \ell'_m \rangle = \sum_{k \neq c}^K \mathbf{p}_{n, k} \mathbf{p}_{m, k} + (\mathbf{p}_{n, c} - 1)(\mathbf{p}_{m, c} - 1) \geq 0 \quad (6)$$

According to Fact 1, we prove the theorem. \square

B ALGORITHMS OF ONLINE MEMORY UPDATE

We provide the details of online ring buffer update and Balanced Experience Replay (BER) in Alg. 1 and Alg. 2, respectively. We directly add all seen classes into the memory buffer without a separate buffer for the current batch of data stream. The memory buffer allocated for current task works like a sliding window of the data stream. In this case, one sample may not be seen only once as long as it

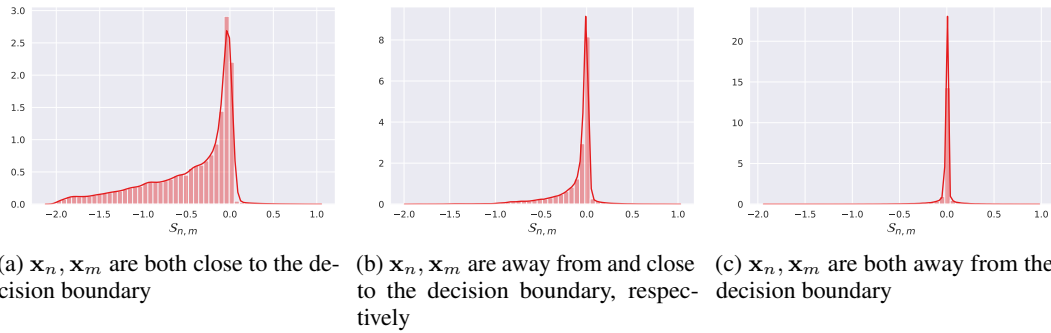


Figure 6: Distribution of $\mathcal{S}_{n,m} = \langle \ell'_n, \ell'_m \rangle$ for a 5-class task under the assumptions: (a) the two samples are close to the decision boundary of their true classes and the model is reasonably trained, i.e. $\mathbf{p}_n, \mathbf{p}_m$ concentrate on two classes; (b) the model just gives random guessing, i.e. $\mathbf{p}_n, \mathbf{p}_m$ are uniformly distributed.

Algorithm 1 Ring Buffer Update with Fixed Budget

Input: \mathcal{B} - current data batch of the data stream, \mathcal{C}_b - the set of classes in \mathcal{B} , \mathcal{B}_c - samples of class c in \mathcal{B} , \mathcal{M} - memory buffer, \mathcal{C}_m - the set of classes in \mathcal{M} , \mathcal{M}_c - samples of class c in \mathcal{M} , K - memory buffer size.

```

for  $c$  in  $\mathcal{C}_b$  do
  if  $c$  in  $\mathcal{C}_m$  then
     $\mathcal{M}_c = \mathcal{M}_c \cup \mathcal{B}_c$ 
  else
     $\mathcal{M}_c = \mathcal{B}_c$ ,  $\mathcal{C}_m = \mathcal{C}_m \cup \{c\}$ 
  end if
end for
 $R = |\mathcal{M}| + |\mathcal{B}| - K$ 
while  $R > 0$  do
   $c' = \arg \max_c |\mathcal{M}_c|$ 
  remove the first sample in  $\mathcal{M}_{c'}$ ,  $R = R - 1$ 
end while
return  $\mathcal{M}$ 

```

Algorithm 2 Balanced Experience Replay

Input: \mathcal{M} - memory buffer, \mathcal{C} - the set of classes in \mathcal{M} , \mathcal{M}_c - samples of class c in \mathcal{M} , B - training batch size, Θ - model parameters, \mathcal{L}_Θ - loss function w.r.t. Θ , \mathcal{B}_t - latest batch from the data stream.

```

 $\mathcal{M} \leftarrow \text{MemoryUpdate}(\mathcal{B}_t)$ 
 $n_c = \lfloor B/|\mathcal{C}| \rfloor$ ,  $r_c = B \bmod |\mathcal{C}|$ 
 $\mathcal{C}_r \stackrel{r_c}{\sim} \mathcal{C} \triangleleft$  sample  $r_c$  classes from all seen classes without replacement.
 $\mathcal{B}_{train} = \emptyset$ 
for  $c$  in  $\mathcal{C}$  do
  if  $c$  in  $\mathcal{C}_r$  then
     $n_c = n_c + 1$ 
  end if
   $\mathcal{B}_c \stackrel{n_c}{\sim} \mathcal{M}_c \triangleleft$  sample  $n_c$  samples from  $\mathcal{M}_c$ 
   $\mathcal{B}_{train} = \mathcal{B}_{train} \cup \mathcal{B}_c$ 
end for
 $\Theta \leftarrow \text{Optimizer}(\mathcal{B}_{train}, \Theta, \mathcal{L}_\Theta)$ 

```

stays in the memory buffer, as we draw training batches from the memory buffer instead of directly from the data stream. This strategy is a more efficient use of the memory buffer when $|\mathcal{B}| < n_c$, where $|\mathcal{B}|$ is the batch size of current data (i.e. the number of new samples added into the memory buffer at each iteration), we set $|\mathcal{B}|$ to 1 or 2 in our experiments (see Appx. D for a discussion of this). Note that we update samples in the memory based on its task ID instead of class ID for permuted tasks, as in this case each task always includes the same set of classes.

C EXTRA EXPERIMENT RESULTS

To verify if BER do reduce the diversity of gradients, we compare the distributions of similarities of gradients and representations with/without DRL by training a model on Disjoint MNIST tasks (refer to Sec. 4). Fig. 7a shows the changes to similarities of representations caused by DRL, the similarities from different classes notably shifting towards a smaller region, as expected. Interestingly, similarities from the same class also shift slightly towards a smaller region. Accordingly, the similarities of gradients from different classes are more concentrated around 0, whilst the similarities from the same class are shifted towards 0 (Fig. 7b). We interpret this as the generalization between different classes can also prevent overfitting of individual classes.

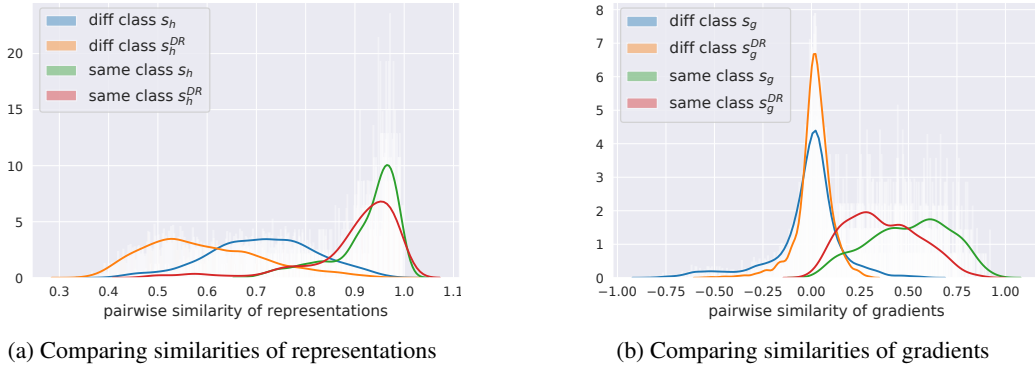


Figure 7: Distributions of similarities of gradients and representations with/without DRL. s_h^{DR} and s_h denote similarities of representations with and without DRL, respectively, s_g^{DR} and s_g denote similarities of gradients with and without DRL, respectively.

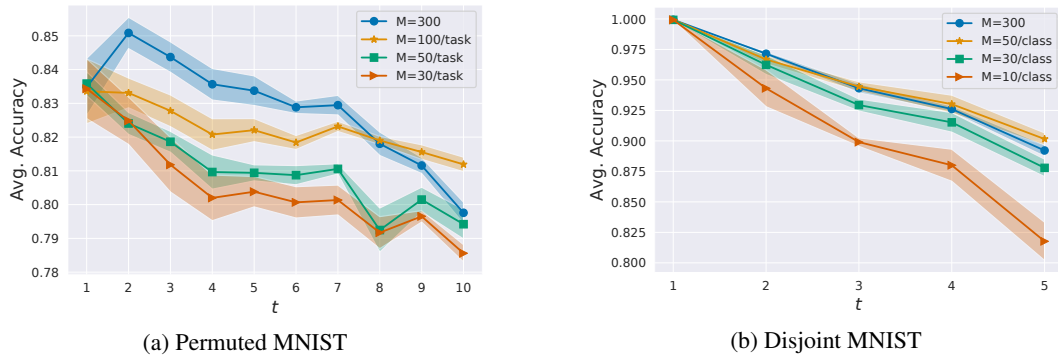


Figure 8: Average accuracy of DRL+BER with different memory sizes. The x axis is the index of tasks, the shaded area is plotted by standard deviation of 5 runs.

Table 6: Training time (in seconds) of the whole task sequence of CIFAR tasks, which have been tested on a device with one NVIDIA TITAN V GPU.

	DRL+BER	BER	ER	A-GEM	GSS-greedy
CIFAR-10	258.6 ± 0.4	249.1 ± 0.8	247.0 ± 0.7	5209.8 ± 3.7	816.6 ± 44.0
CIFAR-100	1150.8 ± 8.0	1121.6 ± 4.0	1029.1 ± 10.3	5162.2 ± 48.1	3731.9 ± 30.0

Fig. 8 compares average accuracy of DRL+BER on MNIST tasks with different memory sizes. It appears the fixed memory size is more efficient than the incremental memory size. For example, the fixed memory size ($M = 300$) getting very similar average accuracy with memory $M = 50$ per class in Disjoint MNIST while it takes less cost of the memory after task 3. Meanwhile, the fixed memory size ($M = 300$) gets much better performance than $M = 50$ per task in most tasks of Permuted MNIST and it takes less cost of the memory after task 6. Since the setting of fixed memory size takes larger memory buffer in early tasks, the results indicate better generalization of early tasks can benefit later tasks, especially for more homogeneous tasks such as Permuted MNIST. The results also align with findings about Reservoir sampling (which also has fixed buffer size) in Chaudhry et al. (2019b) and we also believe a hybrid memory strategy can obtain better performance as suggested in Chaudhry et al. (2019b).

Tab. 6 compares the training time of CIFAR tasks. As we use ResNet18 for CIFAR tasks, the number of model parameters is much larger than the dimension of representations. Consequently, A-GEM and GSS-greedy take much more time on training than other methods because they rely on inner product of parameters' gradients.

Table 7: Accuracy of each task of Disjoint CIFAR-100 at the end of the data stream

	DRL+BER	BER	ER	A-GEM	GSS-greedy
task 1	0.133 ± 0.016	0.064 ± 0.008	0.06 ± 0.008	0.079 ± 0.041	0.317 ± 0.02
task 2	0.089 ± 0.006	0.023 ± 0.007	0.026 ± 0.005	0.017 ± 0.011	0.008 ± 0.002
task 3	0.169 ± 0.015	0.086 ± 0.008	0.051 ± 0.008	0.023 ± 0.02	0.025 ± 0.012
task 4	0.096 ± 0.016	0.022 ± 0.004	0.014 ± 0.004	0. ± 0.	0.013 ± 0.003
task 5	0.138 ± 0.028	0.054 ± 0.006	0.04 ± 0.011	0. ± 0.	0.017 ± 0.003
task 6	0.157 ± 0.016	0.062 ± 0.022	0.055 ± 0.01	0.033 ± 0.03	0.033 ± 0.01
task 7	0.221 ± 0.015	0.136 ± 0.015	0.131 ± 0.015	0.002 ± 0.003	0.091 ± 0.017
task 8	0.202 ± 0.011	0.12 ± 0.021	0.124 ± 0.012	0.011 ± 0.012	0.081 ± 0.016
task 9	0.197 ± 0.011	0.163 ± 0.009	0.08 ± 0.028	0. ± 0.	0.092 ± 0.025
task 10	0.09 ± 0.017	0.466 ± 0.014	0.428 ± 0.035	0.129 ± 0.075	0.451 ± 0.026
Avg.	0.149 ± 0.006	0.119 ± 0.007	0.1 ± 0.006	0.029 ± 0.009	0.117 ± 0.004

Table 8: Learning rate of different methods in different tasks

	Permuted MNIST	Disjoint MNIST	Disjoint CIFAR-10	Disjoint CIFAR-100
DRL+BER	0.0004	0.0002	0.0001	0.0001
BER	0.0004	0.0002	0.0001	0.0001
ER	0.0004	0.0002	0.0001	0.0001
A-GEM	0.0004	0.0001	0.0002	0.00005
GSS-greedy	0.05	0.05	0.01	0.01

Tab. 7 compares the final accuracy of each task of Disjoint CIFAR-100. We can see that DRL+BER achieves a more balanced performance over all learned tasks than other methods, i.e. it obtains much better performance on tasks in the middle of the sequence. In comparison, BER gets highest accuracy on the latest task, GSS-greedy obtains the highest accuracy on the first task and a relatively high accuracy on the last task. ER demonstrates similar properties with BER but a bit lower accuracy of most tasks. A-GEM has failed to get a reasonable performance in the end. DRL+BER gets the highest average accuracy in the end, but it gets the lowest accuracy of the last task, meaning it loses more elasticity than other methods in the end of the task sequence. We can see there is a trade-off between remembering old tasks and learning a new task. We believe such trade-off also depends on the model’s capacity and the difficulty of the task sequence. It is unlikely to have a model which is able to learn infinite task sequence. A practical solution could combine the strength of different approaches, such as utilising small episodic memories and growing the model incrementally.

D HYPER-PARAMETERS IN EXPERIMENTS

To obtain competitive performance of all methods, we use following settings, and hyper-parameters are chosen by grid search on validation sets: *i)* The configurations of GSS-greedy are as the same as suggested in Aljundi et al. (2019), with batch size set to 10 and each batch receives multiple iterations, the optimizer is Stochastic Gradient Descent (SGD). *ii)* For the other methods, we use the ring buffer memory as described in Sec. 3, the batch size of current data is set to 2 for Disjoint CIFAR-100 and 1 for other tasks; each batch only receives one iteration. We use Adam (Kingma & Ba, 2014) as the gradient optimizer as it shows improved performance in most cases. *iii)* The hyperparameter λ of DRL (Eq. (4)) is set to $1e^{-3}$, $1e^{-4}$, $2e^{-4}$, $1e^{-5}$ for Permuted MNIST, Disjoint MNIST, Disjoint CIFAR-10, and Disjoint CIFAR-100, respectively. More details of experimental settings are provided in the supplementary material.

In the setting of limited training set size in online learning, we either use a small batch size or iterate on one batch several times to obtain necessary steps for gradient optimization. We chose a small batch size with one iteration instead of larger batch size with multiple iterations, as by our memory update strategy (Sec. 3) it achieves similar performance with fewer hyperparameters. Since GSS-greedy

has a different strategy for updating memories, we leave it at its default settings. We chose Adam optimizer Kingma & Ba (2014) instead of SGD for most of the methods, since the gradients produced by small data batches display high variance, especially in the online setting. Adam copes with this issue better than SGD, as its update stepsize is governed by the learning rate and a term analogous to the Signal to Noise Ratio (SNR) instead of the latest gradient: $\Delta_k \approx \alpha \cdot \hat{m}_k / \sqrt{\hat{v}_k}$, where \hat{m}_k and \hat{v}_k denotes the moving approximation of the first and second moments at the k -th iteration, respectively. Adam generally gains better or similar performance to SGD for most of the methods except for GSS-greedy. We believe this is the reason that the results of A-GEM and ER reported in this paper are superior to those reported in related papers. In GSS-greedy, the samples of current task in the training batch are unchanged for several iterations. In this case, Adam can easily overshoot, as $\hat{m}_k / \sqrt{\hat{v}_k}$ will shift to 1, and hence push Δ_k to the maximum step-size. For this reason, we used the SGD optimizer for GSS-greedy with its default settings.

Other hyperparameters are as following:

1. The training batch size is 20 for the tasks in Permuted MNIST and Disjoint CIFAR-100, and 10 for Disjoint MNIST and Disjoint CIFAR-10.
2. For A-GEM the batch size of generating the reference gradient is 256 for tasks of MNIST and CIFAR-10, and 1500 for tasks of CIFAR-100.
3. The learning rate of all cases are shown in Tab. 8, whereas GSS-greedy uses SGD optimizer and others use Adam.